

**Flow dynamics
around downwelling
submarine canyons**

J. M. Spurgin and
S. E. Allen

Flow dynamics around downwelling submarine canyons

J. M. Spurgin and S. E. Allen

Department of Earth, Ocean and Atmospheric Sciences, University of British Columbia, Vancouver, British Columbia, Canada

Received: 8 May 2014 – Accepted: 9 May 2014 – Published: 23 May 2014

Correspondence to: J. M. Spurgin (jspurgin@eos.ubc.ca)

Published by Copernicus Publications on behalf of the European Geosciences Union.

Title Page

Abstract

Introduction

Conclusions

References

Tables

Figures



Back

Close

Full Screen / Esc

Printer-friendly Version

Interactive Discussion



Abstract

Flow dynamics around a downwelling submarine canyon were analysed with the Massachusetts Institute of Technology general circulation model. Blanes Canyon (North-west Mediterranean) was used for topographic and initial forcing conditions. Fourteen scenarios were modelled with varying forcing conditions. Rossby number and Burger number were used to determine the significance of Coriolis acceleration and stratification (respectively) and their impacts on flow dynamics. A new non-dimensional parameter (χ) was introduced to determine the significance of vertical variations in stratification. Some simulations do see brief periods of upwards displacement of water during the 10 day model period, however, the presence of the submarine canyon is found to enhance downwards advection of density in all model scenarios. High Burger numbers lead to negative vorticity and a trapped anticyclonic eddy within the canyon, as well as an increased density anomaly. Low Burger numbers lead to positive vorticity, cyclonic circulation and weaker density anomalies. Vertical variations in stratification affect zonal jet placement. Under the same forcing conditions, the zonal jet is pushed offshore in more uniformly stratified domains. Offshore jet location generates upwards density advection away from the canyon, while onshore jets generate downwards density advection everywhere within the model domain. Increasing Rossby values across the canyon axis, as well as decreasing Burger values, increase negative vertical flux at shelf break depth (150 m). Increasing Rossby numbers lead to stronger downwards advection of a passive tracer (nitrate) as well as stronger vorticity within the canyon. Results from previous studies were explained within this new dynamic framework.

1 Introduction

Submarine canyons are features typical of continental slopes and deeply incise the continental shelf. On a regional scale, physical processes (such as upwelling and cross-shelf exchange) can be modified/enhanced due to the presence of a submarine

OSD

11, 1301–1356, 2014

Flow dynamics around downwelling submarine canyons

J. M. Spurgin and
S. E. Allen

Title Page

Abstract

Introduction

Conclusions

References

Tables

Figures

◀

▶

◀

▶

Back

Close

Full Screen / Esc

Printer-friendly Version

Interactive Discussion



the canyon (with positive anomalies both upstream and downstream of the canyon in the slope region).

In simulations with a trapped anticyclone or negative vorticity, differences occur between studies. Under constant downwelling winds, a strong anticyclone within a canyon (in the upper 200 m) and small net cross-shore exchanges are driven by vortex compression or frictional coupling to alongshore flow (She and Klinck, 2000). Vertical flux is downwards everywhere over the canyon at shelf break depth (ibid). Observations over Blanes Canyon reveal that flow near the shelf break follows isobaths along canyon walls, with weak circulation in the canyon head (Flexas et al., 2008). In the upper 100 m, circulation is cyclonic along the canyon mouth, but weakly anticyclonic within the canyon. Vertical velocity estimates reveal net downwards transport in the upper 100 m, but net upwards transport from 100–200 m (Flexas et al., 2008). Density sections suggest local downwelling/upwelling occurs along the upstream/downstream canyon walls between 100 to 200 m depth (ibid).

In the studies of downwelling submarine canyons, there does not appear to be a clear agreement on flow dynamics (Table 1). This study attempts to better understand these and other differences between previous studies, as well as resolve the parameters that drive general flow dynamics in downwelling submarine canyons. The specific objectives of this study are: (1) determine if upwelling occurs in or around downwelling canyons and (2) determine what parameters affect flow dynamics. Particularly, which parameters impact horizontal circulation, vertical transport, density advection and passive tracer advection.

For the purpose of this study, canyon topography is based on the bathymetry of Blanes Canyon (BC) (Fig. 1). BC lies along the Catalan coast, in the northwest Mediterranean Sea and is one of the few submarine canyons for which there have been multiple observational and numerical studies. The core simulation is a model of BC, which replicates observations of Flexas et al. (2008). However, simulations of Klinck (1996); She and Klinck (2000) and Skliris et al. (2001, 2002) are also replicated and 9 other

Flow dynamics around downwelling submarine canyons

J. M. Spurgin and
S. E. Allen

Title Page

Abstract Introduction

Conclusions References

Tables Figures

◀ ▶

◀ ▶

Back Close

Full Screen / Esc

Printer-friendly Version

Interactive Discussion



simulations with variations in flow, stratification, topography and boundary conditions were modelled.

Section 2 describes the numerical model, domain bathymetry, parameter choices, modelled cases, and analysis calculations. Section 3 details results for all model simulations. Section 4 discusses the impacts of various parameters to modelled dynamics. Section 5 examines the significance of the results.

2 Model

2.1 Model description

Simulations were run with the Massachusetts Institute of Technology general circulation model (MITgcm) (Adcroft et al., 2004). The model is rooted in incompressible Navier–Stokes equations; non-hydrostatic terms were used for all simulations.

2.2 Domain and canyon bathymetry

The model domain is 120 km in the alongshore (x direction), 90 km in the cross-shore (y direction), and 1200 m in the vertical (z direction) (Fig. 1). Positive x points upstream (eastward), positive y points onshore (northward), and positive z points upwards.

Minimum ocean depth is 20 m and stretches for ~ 20 km in the cross-shore (hereafter referred to as the inner shelf). Between the inner shelf and shelf break lies the outer shelf; in this region depth drops to 150 m over 20 km. The slope extends from the shelf break (150 m) to an abyssal depth of 1200 m, and extends over 25 km in the cross-shore. The canyon topography was based on Blanes Canyon bathymetry shown by Flexas et al. (2008). Geometric parameters were kept nearly constant in all model simulations (Table 2).

Flow dynamics around downwelling submarine canyons

J. M. Spurgin and
S. E. Allen

Title Page

Abstract

Introduction

Conclusions

References

Tables

Figures

◀

▶

◀

▶

Back

Close

Full Screen / Esc

Printer-friendly Version

Interactive Discussion



2.3 Parameter specifications

Temperature, salinity, and nitrate stratification in the model were based on data from the National Virtual Ocean Data System (NVOADS, <http://ferret.pmel.noaa.gov/NVOADS/UI.vm>). Measured values at various depths of temperature and salinity were collected from the World Ocean Atlas 2005 $1^\circ \times 1^\circ$ monthly means at approximately 40.5°N , 2.5°E . Values for nitrate were collected from annual means of the same data set at the same position. For high vertical resolution runs, values between data points were linearly interpolated. A linear equation of state was applied, with a thermal expansion coefficient of $2.0 \times 10^{-4} \text{ (}^\circ\text{C}^{-1}\text{)}$ and a haline contraction coefficient of 7.4×10^{-4} .

Horizontal resolution varies in alongshore and cross-shore directions, grid spacing is $\sim 1 \text{ km}$ along each boundary and decreases linearly to 200 m over the canyon. Overall, there is 200 m horizontal spacing between 33 km to 87 km in the alongshore, and 20 km to 80 km in the cross-shore. Ninety vertical layers are concentrated around the top of the domain, and vertical spacing ranges from 5 m (in the upper 200 m) to 20 m (everywhere below 200 m).

The Coriolis parameter was assumed constant ($f = 1.0 \times 10^{-4} \text{ s}^{-1}$). Bottom friction was parameterized with a quadratic drag coefficient of 2.0×10^{-3} . A vertical eddy viscosity of $1.0 \times 10^{-2} \text{ m}^2 \text{ s}^{-1}$ was applied. The model used non-hydrostatic equation sets, with a time step of 40 s for all runs. Viscous (i.e. no-slip) conditions were applied at the sides and bottom of the domain, and an implicit free surface was used. Heat and salt were laterally and vertically diffused with a Laplacian diffusivity of $1 \times 10^{-7} \text{ m}^2 \text{ s}^{-1}$. A Smagorinsky harmonic viscosity factor (Smagorinsky, 1963) of 2.2 was applied (as recommended in Griffies and Hallberg, 2000). All tracers (i.e. temperature, salinity, and nitrate) were advected in time using a 3rd order direct space-time with flux limiting scheme.

All model scenarios had a closed (no-slip) boundary along the coastal boundary. The offshore boundary was open with an Orlanski (1976) radiation condition applied.

OSD

11, 1301–1356, 2014

Flow dynamics around downwelling submarine canyons

J. M. Spurgin and
S. E. Allen

Title Page

Abstract

Introduction

Conclusions

References

Tables

Figures

◀

▶

◀

▶

Back

Close

Full Screen / Esc

Printer-friendly Version

Interactive Discussion



All but 2 simulations used periodic alongshore conditions; these two simulations will be explained further in the next section.

2.4 Model simulations

All modelled scenarios were forced by applying a wind stress and/or body force over the domain. A body force was applied as an additional forcing to the momentum equations (Dawe and Allen, 2010). Fourteen scenarios were modelled based on minor changes in either domain stratification or forcing (Tables 3 and 4). Two non-dimensional parameters were calculated to highlight incoming velocity (Rossby number, R_o):

$$R_o = \frac{U}{fL} \quad (1)$$

and stratification (Burger number, B_u):

$$B_u = \frac{N_{sb}H_{sb}}{fW}. \quad (2)$$

Dynamic parameters are incoming velocity, U , the Coriolis parameter, f , and stratification characterised by the buoyancy frequency at shelf break depth (150 m), N_{sb} . Geometric parameters are length of the canyon, L , depth at the shelf break, H_{sb} , and width across mid-canyon, W .

To better understand the impact changes in stratification have on flow dynamics, a third parameter, a non-dimensional measure of vertical stratification, χ , was introduced. This new parameter measured uniformity of stratification and was calculated as the change in buoyancy frequency (N) divided by the average buoyancy frequency near shelf break depth:

$$\chi = \Delta N(z) [\overline{N}(z)]^{-1}, \quad (3)$$

where $N(z)$ is measured over a length scale of ± 75 m from the shelf break and $\overline{N}(z)$ is the average stratification over the length scale. Negative χ values indicate stronger stratification in the shallower layers.

Flow dynamics around downwelling submarine canyons

J. M. Spurgin and
S. E. Allen

Title Page

Abstract

Introduction

Conclusions

References

Tables

Figures

◀

▶

◀

▶

Back

Close

Full Screen / Esc

Printer-friendly Version

Interactive Discussion



Flow dynamics around downwelling submarine canyons

J. M. Spurgin and
S. E. Allen

Title Page

Abstract

Introduction

Conclusions

References

Tables

Figures

◀

▶

◀

▶

Back

Close

Full Screen / Esc

Printer-friendly Version

Interactive Discussion



In addition, placement of incoming coastal jets varied, vertically and horizontally, in previous studies (Table 4). These were recreated to ensure the dynamics of the original studies were reproduced.

Core model simulations were based on the Flexas et al. (2008) observations.

The first scenario (uniform wind, **UW**) consisted of a uniform wind stress ($\tau = -0.0626 \text{ N m}^{-2}$) to drive a current along the surface, and a body forcing (applied near shelf break depth) to drive a current along the shelf break (similar to the Northern Current seen in the Mediterranean Sea). The current was accelerated over the first two model days, and then held at a “steady” state for the remainder of the simulation (“steady” state indicates maximum flow velocity never varied more than 20 %).

The second scenario (opposing wind, **OW**) consisted of two opposing wind stresses to drive surface flow, and a slightly stronger body forcing to drive the shelf break current. This setup was used to reproduce eastward flow seen over the continental shelf (Flexas et al., 2008). To match the offshore distance of the eastward flow, wind stresses were applied such that the offshore two-thirds of the domain had a wind stress of $\tau = -0.0626 \text{ N m}^{-2}$ and the nearshore one-third of the domain had a wind stress of $\tau = +0.0376 \text{ N m}^{-2}$. Again, the current was increased during the first two model days.

Additional scenarios were modelled to either recreate flow dynamics seen in previous numerical studies (3 scenarios) or investigate other impacts to flow dynamics (9 scenarios).

A Klinck-like (**KL**) scenario was modelled using a uniform stratification ($N = 0.0016 \text{ s}^{-1}$) and a flat shelf at 150 m (topography everywhere else in the domain remained the same) (Klinck, 1996). A mostly uniform flow was reproduced by removing all wind stress and y-dependence in the body forcing. However, flow over the flat shelf was weaker relative to flow along the continental shelf and over the open ocean. Speed of the body forcing was reduced to create a zonal velocity of about 10 cm s^{-1} .

A Skliris-like (**SK**) simulation had uniform stratification over three regions: (1) the upper 20 m ($N = 6.0 \times 10^{-3} \text{ s}^{-1}$); (2) from 20 m to 120 m ($N = 1.5 \times 10^{-3} \text{ s}^{-1}$); (3) from 120 m to bottom depth ($N = 0.5 \times 10^{-3} \text{ s}^{-1}$) (Skliris et al., 2001). Wind stress was

removed, but y dependence on body forcing was kept. Body forcing was reduced to create a maximum zonal velocity of approximately 7 cm s^{-1} .

To simulate the She and Klinck (2000) study, a constant weak body forcing was applied over the upper 40 m, generating a maximum zonal speed of $\sim 13 \text{ cm s}^{-1}$ (**She**).

Stratification was varied over the entire depth, based on the equation for density provided in the original study. Initial fields are temperature (T):

$$T(z, t = 0) = 10 \text{ }^\circ\text{C} - 0.5 \text{ }^\circ\text{C} \exp\left(\frac{z}{110 \text{ m}}\right) \quad (4)$$

and salinity (S):

$$S(z, t = 0) = 33 - 0.5 \exp\left(\frac{z}{110 \text{ m}}\right), \quad (5)$$

where z is depth below 0 and measured in metres.

To better understand the impact of open vs. periodic boundary conditions, two scenarios with open alongshore boundaries were modelled. In these simulations, Orlanski radiation conditions were applied across both alongshore boundaries and the offshore boundary. The first scenario (open boundary conditions, **OBC**) has the same geometry as the UW case, but both wind stress and body forcing were increased to recreate a similar zonal flow field as seen in the UW simulation. The second simulation (slanted topography, **ST**) used geometry that was similar to real world Blanes Canyon bathymetry (i.e. a slanted coastline and curvature within the canyon). Forcing in this scenario was the same as the OBC case.

Two scenarios of constant surface forced (**SF**) flow were modelled, one forced by a wind stress and one forced with a surface body force applied to the upper 30 m. Results from these simulations were very similar, and will therefore be discussed as one example.

A uniform stratification (**US**) scenario was modelled with the same geometry and forcing as the UW scenario, but stratification from the Klinck-like case was used ($N = 0.0016 \text{ s}^{-1}$ everywhere). Similarly, a high Burger number (**HB**) scenario was modelled.

Flow dynamics around downwelling submarine canyons

J. M. Spurgin and
S. E. Allen

Title Page

Abstract

Introduction

Conclusions

References

Tables

Figures

◀

▶

◀

▶

Back

Close

Full Screen / Esc

Printer-friendly Version

Interactive Discussion



mouth; one in the upstream (V2) and one in the downstream (V3). Again, flux was calculated from surface to shelf break depth. Finally, two planes were used to calculate vertical flux at shelf break depth. These planes extend from the canyon head to canyon mouth and split across the canyon axis (upstream = W1, downstream = W2).

5 Net vertical flux was calculated by summing flux across these two planes. Flux across all planes was found by multiplying velocity of each grid cell by area of each grid cell and summing over the entire plane.

Relative vorticity in the basin can be expressed as:

$$10 \quad \zeta = \frac{\delta V}{\delta x} - \frac{\delta U}{\delta y}, \quad (6)$$

where ζ is the vertical component of vorticity, V is the meridional velocity, and U is zonal velocity. Absolute vorticity was measured as the relative vorticity divided by Coriolis parameter, f .

15 Average zonal velocity across the canyon axis at shelf break depth (150 m) was used to calculate a second Rossby number ($R_{\bar{U}_{\text{can}}}$). This velocity is calculated as:

$$\bar{U}_{\text{can}} = \frac{\sum U(y)\Delta y}{L}, \quad (7)$$

20 where U is taken as the zonal velocity in each meridional grid point that lies along the canyon axis, and Δy is the horizontal distance the zonal velocity is applied. A canyon Rossby number was calculated as:

$$R_{\bar{U}_{\text{can}}} = \frac{\bar{U}_{\text{can}}}{fL}. \quad (8)$$

25 Density was calculated for all model simulations as average density in the canyon across the shelf break plane (W1 and W2). This value was averaged during the approximate advection dominated phase (averaged from model day 4–10). Average density was subtracted from initial density at shelf break depth to give an average density anomaly in the canyon.

Flow dynamics around downwelling submarine canyons

J. M. Spurgin and
S. E. Allen

Title Page	
Abstract	Introduction
Conclusions	References
Tables	Figures
◀	▶
◀	▶
Back	Close
Full Screen / Esc	
Printer-friendly Version	
Interactive Discussion	



Changes in density difference within the canyon relative to away from the canyon were determined by calculating a density difference anomaly. This anomaly was found by subtracting a background density difference (calculated as a 5 grid point average along the downstream boundary) from the difference at grid points of similar isobaths:

$$\rho_{\text{anom}} = \rho_{\text{difference}}(x_i, y_j, z) - \rho_{\text{boundary}}(y_j, z), \quad (9)$$

where x_i and y_j are alongshore and cross-shore points (respectively) that are ± 5 m of the isobath used to calculate the background density difference ($\rho_{\text{boundary}}(y_j, z)$).

Nitrate concentration was used as a passive tracer in the model. An average nitrate concentration was also calculated as the average nitrate value in the canyon across the shelf break plane (W1 and W2) during the advection dominant phase (model days 4–10). The average nitrate concentration is subtracted from the initial nitrate concentration at shelf break depth to give an average nitrate anomaly in the canyon.

3 Results

3.1 Flow evolution

All model scenarios show an initial time-dependent response to model forcing, similar to that described by Allen and Durrieu de Madron (2009), which lasts approximately two to three days (Fig. 3). During this phase, zonal and vertical flux exhibit a negative ramping everywhere in the domain. In all but two simulations, vertical flux across the downstream plane (W2; Fig. 2) reverses at approximately day 1, and continues towards a maximum positive value by day 2–2.5. In these simulations, magnitude of meridional flux over the canyon gently increases across both planes, being positive (onshore) in the upstream (V2; Fig. 2) and negative (offshore) in the downstream (V3; Fig. 2) until reaching a maximum near the end of the time-dependent phase. In the simulations with a coastal jet (She and SF), vertical flux is downwards across both the upstream and downstream planes until day 1 (Fig. 3b). After this, negative flux across the downstream

Flow dynamics around downwelling submarine canyons

J. M. Spurgin and
S. E. Allen

Title Page

Abstract

Introduction

Conclusions

References

Tables

Figures



Back

Close

Full Screen / Esc

Printer-friendly Version

Interactive Discussion



plane weakens in time, while negative flux across the upstream plane continues to strengthen. For these scenarios, upstream onshore flux and downstream offshore flux strengthen during the model simulation.

The time-dependent phase is followed by an advection dominated phase. During this phase, zonal flux stays within approximately 2–17% of the maximum value reached during the time-dependent phase for most simulations. Meridional flux also gently fluctuates, always being positive in the upstream and negative in the downstream for all model scenarios. The two surface forced simulations (She and SF) show a zonal flux that continuously increases during the model simulation, with a final zonal flux that is approximately 50% stronger than flux at the end of the time-dependent phase (Fig. 3b). This indicates neither scenario may be reaching an advection dominated phase.

Vertical flux time dependence varies between model simulations, with 3 primary patterns emerging. Firstly, vertical flux varies between positive and negative transport over both the upstream and downstream plane of the canyon, with flux values being roughly the same in the upstream/downstream (Fig. 3a). This pattern is seen in the UW and OW simulations. Secondly, flux across the upstream plane is mirrored across the downstream plane, i.e. as magnitude across one plane increases, magnitude across the other plane increases well (Fig. 3c). In 6 simulations (ST, KL, SK, US, HB, SHR) this pattern occurs with upstream transport always positive and downstream transport always negative. In 4 runs (OBC, LRC, BLRB, KHRB) the above pattern occurs, but flux across the upstream/downstream planes does cross between positive and negative values during model days 4–6. Thirdly, simulations with a coastal jet (She and SF) exhibit strengthening negative flow across the upstream plane and weakening negative flow across the downstream plane (Fig. 3b). In the She case, flux across the downstream plane becomes positive around model day 4. In the SF case, flux over the upstream plane begins to weaken around model day 7.

To ensure aliasing is not occurring with 12 h model output, another 10 day UW simulation was run with model output written every 3 h (Spurgin, 2014). Small differences

Flow dynamics around downwelling submarine canyons

J. M. Spurgin and
S. E. Allen

[Title Page](#)[Abstract](#)[Introduction](#)[Conclusions](#)[References](#)[Tables](#)[Figures](#)[Back](#)[Close](#)[Full Screen / Esc](#)[Printer-friendly Version](#)[Interactive Discussion](#)

in flux estimates are seen during the time-dependent phase. Differences during the advection-dominant phase are less than 10%.

3.2 Circulation in the canyon

Model simulations exhibit three types of horizontal circulation: (1) formation of an anti-cyclonic eddy within the canyon, (2) cyclonic circulation everywhere within the canyon and (3) weak circulation everywhere within the canyon. The evolution of the first two horizontal flow patterns are discussed below. Firstly, the anticyclonic circulation is detailed, followed by a description of the cyclonic circulation.

For high Burger number simulations (particularly, UW, OW, OBC, ST, HB, KHRB) horizontal flow during the time-dependent phase is cyclonic over the canyon (Fig. 4a, left). Toward the end of this phase, flow along the downstream rim becomes stronger relative to the upstream rim (Fig. 4b, left). After one more model day (by day 3), flow in the canyon head becomes anticyclonic and this pattern persists for the remainder of the model simulation (Fig. 4c, left). Vertical velocity during the first day of simulation is negative everywhere in the canyon, and strongest in the upstream. As the flow evolves, a region of positive vertical velocity appears in the downstream half of the canyon and moves toward the downstream corner of the canyon mouth.

During the time-dependent phase, flow becomes faster over the canyon axis and impinges on the downstream wall. Strong downwelling occurs at and above shelf break depth (Fig. 4, left) but decreases with depth. This leads to compression of the isopycnals as they cross the canyon and an anticyclonic eddy forms in the canyon, which persists during the advection dominated phase (Fig. 5a).

For low Burger number simulations (particularly, KL, SK, US, SHR), the cyclonic circulation that forms during the time-dependent phase strengthens as zonal flow accelerates and remains cyclonic (Fig. 4, right and 5b) as downwelling in these cases is quite uniform with depth. Similar to the cases with anticyclonic circulation, vertical flow is negative everywhere within the canyon and strongest in the upstream. However, as the flow evolves, positive vertical velocity begins to appear in the downstream

Flow dynamics around downwelling submarine canyons

J. M. Spurgin and
S. E. Allen

Title Page

Abstract

Introduction

Conclusions

References

Tables

Figures



Back

Close

Full Screen / Esc

Printer-friendly Version

Interactive Discussion



half of the canyon where it remains (it does not get pushed offshore) (Fig. 4, left). For these cases, horizontal flow is strongest along the canyon walls and weaker across the canyon axis (Fig. 5b).

For the purposes of this study, results focus on flow dynamics during the advection dominant phase. Results in the following sections are time-averaged model output. Based on oscillations in the vertical flux time series (Fig. 3), results are averaged from model days 5–8.

3.3 Comparison to previous studies

Current simulations reproduced canyon circulation features seen in previous studies (Table 1). Klinck (1996) was reproduced in the KL simulation. In this low Rossby number, low Burger number and low $|\chi|$ simulation, the cyclonic circulation, antisymmetrical vertical velocity and density change pattern (positive density anomaly outside the canyon mouth) seen in the original study was reproduced in the current model. Similarly, Skliris et al. (2001, 2002) was replicated in the SK simulation. Cyclonic circulation, antisymmetrical vertical velocity and positive density anomalies away from the canyon were reproduced in this low Rossby number, low Burger number, and intermediate $|\chi|$ simulation.

She and Klinck (2000) was mostly reproduced in the She simulation. In this low Rossby number, intermediate Burger number and intermediate $|\chi|$ simulation, net downwards vertical velocity was reproduced. However, a weak cyclonic circulation was seen at all depths in the canyon. This is different from the original study, which saw anticyclonic circulation over the canyon and cyclonic circulation at 300 m and below. Multiple scenarios with varying Rossby, Burger, and $|\chi|$ values (UW, OW, OBC, ST, LRC, SHR) exhibit anticyclonic vorticity at shelf break depth and cyclonic vorticity deeper in the canyon, similar to that seen in She and Klinck (2000). Flexas et al. (2008) was reproduced in the UW and OW simulations. In these high Rossby number, high Burger number, and high $|\chi|$ simulations, the anticyclonic circulation and periods of net positive vertical velocity similar to that seen in the observations were replicated.

Flow dynamics around downwelling submarine canyons

J. M. Spurgin and
S. E. Allen

Title Page

Abstract

Introduction

Conclusions

References

Tables

Figures



Back

Close

Full Screen / Esc

Printer-friendly Version

Interactive Discussion



3.4 Vorticity in the canyon

As previously discussed, all model scenarios either form an anticyclonic eddy in the canyon after the time-dependent phase (Fig. 5a), or have cyclonic circulation in the canyon throughout model simulation (Fig. 5b). Looking at shelf break depth circulation, 6 simulations exhibit an anticyclonic eddy, 4 simulations show cyclonic circulation, and 4 other simulations show weak circulation at this depth.

Simulations with anticyclonic circulation display negative vorticity within the canyon, but opposing positive vorticity along the canyon walls (Fig. 6a). Simulations with cyclonic circulation have the opposite feature, positive vorticity within the canyon, but negative vorticity along canyon walls (Fig. 6b). This reversal of vorticity along bottom topography is due to friction between water parcels and canyon walls. The simulation in which the anticyclonic eddy appears only at a depth below the shelf break (HB) has negative vorticity at shelf break depth (Table 6).

3.5 Upwelling in a downwelling canyon

3.5.1 Vertical velocity

Two main flow patterns are seen in plane views of vertical velocity. In the first pattern, enhanced downwards (upwards) velocity is confined to the upstream (downstream) corner of the canyon mouth at shelf break depth (Fig. 4c, left). This pattern occurs in simulations with weak or negative vorticity at shelf break depth (Table 6). One exception is the HB scenario, which exhibits varying positive and negative vertical velocity patterns everywhere within the canyon (Spurgin, 2014).

In the second vertical flow pattern, vertical velocity presents a more antisymmetric pattern, similar to that seen in previous studies (Klinck, 1996; Skliris et al., 2001, 2002). In these simulations, regions of positive and negative vertical velocity are split along the canyon axis from canyon head to canyon mouth, with negative velocity in the

Flow dynamics around downwelling submarine canyons

J. M. Spurgin and
S. E. Allen

Title Page

Abstract

Introduction

Conclusions

References

Tables

Figures



Back

Close

Full Screen / Esc

Printer-friendly Version

Interactive Discussion



upstream and positive velocity in the downstream (Fig. 4c, right). This pattern occurs in simulations with strong, cyclonic vorticity (Table 6).

In all model scenarios, regions of enhanced upstream negative velocity are stronger than downstream regions of positive velocity. All simulations also exhibit a background negative velocity in regions away from the canyon.

Using the 12 hourly flux time series, periods of positive vertical flux across 3 planes (100, 150, and 600 m) in the canyon (i.e. everywhere between canyon walls from the canyon head to mouth) were calculated over the 10 day model period (Fig. 7). Net upward flux does occur in various downwelling canyon simulations. Note, only 4 scenarios do not see net upwelling at any time (She, SF, SHR, BLRB). Net upwards flux most commonly occurs across the 600 m plane, and least often across the 100 m plane. Periods of net upwards flux mostly occur during the advection dominated phase. The longest occurrence of net upwards flux appears in the OBC simulation, there is a period of net upwards flux that lasts 2.5 model days. Overall, the OBC scenario exhibits the most occurrences of net upwards flux across the 150 and 600 m planes.

3.5.2 Density anomaly

Density anomalies were calculated as density variations (averaged over days 5–8) relative to initial density profiles. Similar to vertical velocity, two distinct anomaly patterns appear. In the first pattern, density anomaly is negative everywhere in the canyon domain (Fig. 8a). At all depths, anomalies are strongest along bottom topography and weaken towards the offshore. This pattern is seen in simulations with a coastal or outer shelf jet (UW, OW, OBC, ST, She, SF, BLRB; Table 7).

In the second pattern, there are strong negative anomalies along bottom topography, but there are also positive anomalies away from the canyon (Fig. 8b). This pattern is seen in simulations with a shelf break or offshore jet (KL, SK, US, HB, LRC, SHR, KHRB); the depth range of positive density anomalies varies (Table 7). For the majority of these simulations, positive anomalies do not extend down to shelf break depth (SK,

Flow dynamics around downwelling submarine canyons

J. M. Spurgin and
S. E. Allen

Title Page

Abstract

Introduction

Conclusions

References

Tables

Figures



Back

Close

Full Screen / Esc

Printer-friendly Version

Interactive Discussion



Flow dynamics around downwelling submarine canyons

J. M. Spurgin and
S. E. Allen

Title Page

Abstract

Introduction

Conclusions

References

Tables

Figures



Back

Close

Full Screen / Esc

Printer-friendly Version

Interactive Discussion



do show regions of both upwards and downwards vertical velocity, however, downwards motion appears to always be dominant. Results of snapshots of net vertical velocity across 3 planes indicate that net upwards displacement of water does occur in the majority of simulations (Fig. 7). In most cases this upwards displacement is brief and commonly occurs at depth. However, the OBC case shows an extended period of net upwards velocity across the 150 m plane from model day 4–6, the beginning of the advection dominated phase. This period of net upwards velocity at shelf break depth is comparable to observations in Flexas et al. (2008). In the current study, a period of net upwelling may be occurring, but the time-mean flow of the advection phase indicates an overall net downwelling.

The prevalence of upwards displacement across the 600 m plane indicates a possible upwelling cell similar to Arduin et al. (1999), in which deep water is upwelled along canyon walls, but returns to the offshore before crossing shelf break depth. Increased stratification has been found to reduce vertical transport (Klinck, 1996). For all current simulations, stratification is weaker with depth, which is likely the reason vertical exchange shows more variation at depth. The irregular occurrences of net upwards displacement across vertical planes, even under semi-steady circulation, indicates observational studies may not be detecting the time-mean flow dynamics occurring in submarine canyons.

Though vertical velocity reveals that upward displacement of water does occur in downwelling canyons, density and nitrate anomalies indicate there is downwards advection of physical properties. Both density and nitrate exhibit regions of positive advection, however these regions occur away from the canyon and positive advection is weaker than negative advection.

Previous studies have found that submarine canyons in downwelling regions enhance coastal downwelling (Klinck, 1996; She and Klinck, 2000; Skliris et al., 2001, 2002). Anomalies of density difference in current simulations show that downwelling is enhanced everywhere within the canyon and over the lower canyon, with downwelling being strongest around the canyon axis. In the upper 100 m, relatively weak

downwelling occurs over the mid-canyon. This region of weaker downwelling appears as a relative lifting of isopycnals from the downstream to upstream canyon rim (Fig. 10). Lifting isopycnals is often a characteristic of upwelling occurring in a region. However, these are instantaneous profiles of what is occurring in the canyon. Using profiles of density difference and density difference anomaly it can be seen that this relative lifting of isopycnals is not actually upwelling, but is a region of relatively weak downwelling.

4.2 Parameter effects

Stratification has been found to have significant impacts on vertical and cross-shore transport (Klinck, 1996). Previous studies have compared forcing responses between weakly and strongly stratified domains. However, these studies use either a uniformly stratified domain (Klinck, 1996), or a domain in which stratification varied in only 3 regions (Skirris et al., 2001, 2002). Other studies have varied stratification in the canyon domain (Arduin et al., 1999; She and Klinck, 2000), but the effects of vertical variation in stratification have never before been studied. Thus, the non-dimensional parameter χ was introduced in this study to investigate the impacts vertical changes in stratification have on flow dynamics. Weak χ values indicate stratification is more uniform in the domain. Negative χ values indicate there is stronger stratification variation at shallower depths. In this section, Rossby number, Burger number, χ values, and incoming jet location are used to determine which regional parameters impact various flow dynamics.

4.2.1 Circulation in the canyon

Patterns in horizontal circulation reveal Burger number to be an important parameter in determining vorticity within the canyon (Fig. 11a). Four simulations with low Burger numbers (SHR, US, SK, KL) exhibit positive vorticity and cyclonic circulation at shelf break depth. Six simulations with high Burger numbers (UW, OW, OBC, ST, HB, KHRB) exhibit negative vorticity and anticyclonic circulation near shelf break depth.

Flow dynamics around downwelling submarine canyons

J. M. Spurgin and
S. E. Allen

Title Page

Abstract

Introduction

Conclusions

References

Tables

Figures



Back

Close

Full Screen / Esc

Printer-friendly Version

Interactive Discussion



Flow dynamics around downwelling submarine canyons

J. M. Spurgin and
S. E. Allen

Title Page

Abstract

Introduction

Conclusions

References

Tables

Figures



Back

Close

Full Screen / Esc

Printer-friendly Version

Interactive Discussion



As the body force is applied to model simulations, an onshore flow occurs and tilts isopycnals downwards. This leads to surface intensification of the zonal jet. Baroclinicity increases with increasing stratification in the upper water column. However, downwelling tends to reduce stratification over the shelf, making the jet more barotropic. With weak near surface stratification (low χ), this leads to an almost barotropic jet which feels bottom friction fairly strongly and is therefore reduced in intensity. In simulations with an offshore jet and low χ values, the zonal velocity is intensified at shelf break depth and negligible along continental slope topography (Table 4; KL, US, HB, LRC, KHRB). Strong near surface stratification (high χ) allows baroclinicity of the jet on the shelf, and thus less friction on it. In simulations with an outer shelf jet and high χ values, zonal velocity is intensified near the surface and negligible along bottom topography (Table 4; UW, OW, OBC, ST, BLRB).

Until now, Rossby number has been based on incoming flow strength. However, a Rossby number based on flow across the canyon axis ($R_{U_{can}}$) may be more appropriate for looking at flow dynamics within the canyon. These values are compared to determine correlations between incoming and canyon axis flow (Fig. 13). Due to the more complex topography in the slanted canyon simulation (ST), it is suspected that $R_{U_{can}}$ is overestimated for this scenario and is thus marked as a possible outlier in subsequent plots.

For simulations with cyclonic circulation at shelf break depth, there is a relatively strong coupling between incoming and canyon axis flow speed. However, for anticyclonic circulation the coupling is weaker. The same incoming Rossby number results in a weaker canyon Rossby number. For the simulations with weak circulation, both Rossby numbers are small and not strongly correlated to each other.

Flow patterns describe the stronger (weaker) coupling between incoming and canyon Rossby numbers in the cyclonic (anticyclonic) simulations. In the anticyclonic cases, the eddy is focused over the canyon axis and flow in the canyon head is towards the upstream, while flow along the mid-canyon is towards the downstream (flow between mid-canyon and canyon mouth is downstream and slightly stronger along the canyon

Flow dynamics around downwelling submarine canyons

J. M. Spurgin and
S. E. Allen

Title Page

Abstract

Introduction

Conclusions

References

Tables

Figures

◀

▶

◀

▶

Back

Close

Full Screen / Esc

Printer-friendly Version

Interactive Discussion

axis) (Fig. 5a). This causes net zonal flow between the canyon head and mid-canyon to be almost negligible and thus weaken overall flow strength across the canyon axis. For cyclonic simulations, zonal flow is weaker across the canyon axis but everywhere towards the downstream (Fig. 5b). Therefore, strong incoming flow increases zonal flow everywhere within the canyon.

For all simulations, Rossby number across the canyon is approximately one-third (or more) lower than Rossby number based on incoming flow. Incoming Rossby number is based on maximum zonal flow at shelf break depth upstream of the canyon, whereas Rossby number across the canyon is integrated from the canyon head to canyon mouth. Thus, incoming Rossby number is slightly overestimated relative to canyon Rossby number.

Downwelling submarine canyons have been observed to modify incoming coastal jets by deflecting the current along canyon walls, with major modifications observed at shelf break depth (Flexas et al., 2008). Current simulations indicate two types of flow deflection occurring, dependent on Burger number. With a low Burger number, flow follows canyon isobaths with strongest flow along bottom topography. With a high Burger number, the flow is more baroclinic and a cut-off anticyclonic eddy forms at shelf-break depth in the canyon.

4.2.2 Vertical flux

Net vertical flux was calculated for all model simulations as net flux in the canyon across the shelf break plane (150 m) averaged during the approximate advection dominated phase (averaged from model days 4–10). Initial errors in net vertical flux were calculated as the difference in flux values during two averaging periods, days 4–10 and days 3–9. However, 2 other sources of error were taken into consideration: (1) error due to variations in zonal flux (which varied 2–17 % for most cases and 50 % for the She and SF simulations); (2) 12 h model output provided an approximate 10 % aliasing error. Therefore, error in all model simulations was taken as the maximum error in: (1) the

sum of the minimum 10% aliasing error plus error due to zonal flux variations or (2) errors in averaging period.

Net vertical flux is directly proportional to Rossby number of flow across the canyon axis and inversely proportional to Burger number (Fig. 14). For example, US and SHR have the highest canyon Rossby number to Burger number ratios, and exhibit the greatest downward flux.

Although previous studies have not specifically looked at changes in zonal flow strength, current simulations show that scenarios with stronger flow across the canyon axis lead to stronger downwards flux. This is unsurprising since increasing Rossby number indicates increasing cross-canyon flow, and thus a stronger pressure gradient along the canyon.

Increased stratification has been found to reduce vertical and cross-shore transport, as well as the depth range which fluid parcels move in a circuit around a canyon (Klinck, 1996; Skliris et al., 2001, 2002). Current simulations show a similar pattern. For example, US and HB cases have the same forcing and variation in stratification, with the only difference being that HB has an increased buoyancy frequency (N). Net cross-shore transport (not shown) in the US (weaker stratification) case is 2× larger and net vertical transport is approximately 6× larger.

Circulation and vertical velocity are instantaneous measurements that capture what is occurring during the advection dominated phase, and both are influenced by Burger and Rossby number. Burger number drives circulation type and strength of vertical flux: simulations with a high Burger number exhibit a trapped anticyclonic eddy and weak vertical flux, simulations with a low Burger number exhibit cyclonic circulation and strong vertical flux. Rossby number drives strength of vertical flux: high Rossby numbers generate strong vertical flux. Thus, Burger and Rossby numbers are important parameters during the advection dominated phase.

Flow dynamics around downwelling submarine canyons

J. M. Spurgin and
S. E. Allen

Title Page

Abstract

Introduction

Conclusions

References

Tables

Figures



Back

Close

Full Screen / Esc

Printer-friendly Version

Interactive Discussion



4.2.3 Density anomalies

Patterns in density anomalies indicate that Burger number (and subsequently vorticity) has the largest impact on the magnitude of density anomalies (Fig. 15). All simulations show net downwards advection of density within the canyon. Simulations with lower Burger numbers (cyclonic circulation) have weaker density anomalies at shelf break depth. Simulations with higher Burger numbers (anticyclonic circulation) exhibit stronger downwards density advection. Simulations with weak circulation also appear to be affected by Burger number.

It is unsurprising that simulations with high Burger numbers have stronger density anomalies. These simulations have stronger variations in initial density between vertical layers. Thus, a water parcel that advects the same vertical distance in a simulation with a high Burger number vs. one with a low Burger number will have a stronger density anomaly. Density anomaly was normalised by the Burger number effect, but showed no relationship to Rossby number, χ or jet location.

Location of incoming zonal jet does affect the occurrence of positive density anomalies in the model domain (Table 7). Simulations with the zonal jet located along the shallow coast or over the outer shelf (directly above the upper canyon) exhibit negative density anomalies (downwards advection) at all depths in the model domain (pattern 1). Simulations which show upwards density advection (positive density anomalies) during the day 5–8 averaged period have a zonal jet located either offshore or along the shelf break. The positive anomalies occur away from the canyon in the upstream and downstream (pattern 2). There is not a correlation between pattern 1/2 and average density anomaly.

Forces can explain how jet location impacts the occurrence of positive density anomalies. For the zonal jet to turn shoreward along the upstream canyon rim, it needs a centrifugal force. This is provided by a change in the pressure gradient: higher pressure offshore of the jet and lower pressure onshore. This weakens the Coriolis force and pressure gradient force balance, and allows flow to turn. In the simulations with an

Flow dynamics around downwelling submarine canyons

J. M. Spurgin and
S. E. Allen

Title Page

Abstract

Introduction

Conclusions

References

Tables

Figures



Back

Close

Full Screen / Esc

Printer-friendly Version

Interactive Discussion



Flow dynamics around downwelling submarine canyons

J. M. Spurgin and
S. E. Allen

Title Page

Abstract

Introduction

Conclusions

References

Tables

Figures



Back

Close

Full Screen / Esc

Printer-friendly Version

Interactive Discussion



offshore or shelf break jet, this pressure gradient change is provided by upwelling of denser water occurring offshore of the canyon and zonal jet (Fig. 8b). For the simulations with a coastal or outer shelf jet, this upwelling occurs over the outer shelf, where stronger downwelling is already occurring. This is seen as a reduction of downwelling rather than upwelling (Fig. 8a).

Previous studies have found that submarine canyons, in regions with a right-bounded jet, enhance the downward advection of density properties (Klinck, 1996; She and Klinck, 2000; Skliris et al., 2001, 2002). Similar results are seen in plots of density difference anomalies (Fig. 8c and d). Downwards advection of density is enhanced within the canyon for all simulations.

4.2.4 Nitrate anomalies

Comparisons of non-dimensional parameters indicate incoming Rossby number has the greatest impact on vertical advection of nitrate (Fig. 16). Simulations with higher Rossby numbers have greater changes in nitrate concentration. This indicates as more flow enters a canyon, advection of passive tracers strengthens. Patterns in incoming Rossby number show a stronger correlation than patterns based on canyon Rossby number.

Density and nitrate anomalies measure a combination of time-dependent and advection dominated downwelling. Density and nitrate anomaly time series for the UW case (not shown) indicate averaged anomalies are approximately 85 % time-dependent and 15 % advection dominated. Allen (1996) finds vertical flux to be inversely proportional to the Burger number for time-dependent upwelling or downwelling. Thus, it would be expected that changes in nitrate advection would be inversely proportional to Burger number. However, this does not occur in current model simulations, e.g. UW and US cases have the same Rossby number, different stratification, but similar nitrate anomalies. Comparing cross-sections of nitrate anomalies (Fig. 9), nitrate anomaly is weaker and broader in the stronger stratification scenario (UW) relative to the weaker stratification scenario (US). The region of negative anomalies upstream of the canyon is

Flow dynamics around downwelling submarine canyons

J. M. Spurgin and
S. E. Allen

Title Page

Abstract

Introduction

Conclusions

References

Tables

Figures

◀

▶

◀

▶

Back

Close

Full Screen / Esc

Printer-friendly Version

Interactive Discussion

approximately 2.5–3× larger in the weaker stratification case (UW). Rossby radius of deformation is 3× larger in the UW case, so size of nitrate anomaly is proportional to Rossby radius (and stratification). Therefore, strength of nitrate anomaly is inversely proportional to stratification, while size of nitrate anomaly is directly proportional to stratification. These have a cancelling effect and only the Rossby number appears to have an influence on nitrate anomaly.

With the exception of the two open boundary simulations, density and nitrate exhibit the same anomaly patterns in the same model scenarios (Table 7): negative anomalies everywhere in the canyon domain (pattern 1) and positive anomalies away from the canyon (pattern 2). This indicates jet location impacts the occurrence of nitrate anomalies following the same reasoning described in the previous section. Therefore, the upwelling occurring away from the canyon includes denser water and higher nitrate concentrations.

Density and nitrate anomalies are integrated measurements and include a strong signal from the time-dependent phase. Anomaly patterns are influenced by jet location, which in turn is affected by vertical variations in stratification. As previously discussed (vertical velocity section), zonal jet placement effects time dependence of vertical flux. Offshore and shelf break jets generate upward velocity away from the canyon and steadier vertical flux (relative to coastal/outer shelf jets). Thus, location of the zonal jet is important during time-dependent phases of flow.

Average diapycnal diffusivity in Ascension Canyon (west coast, North America) has been observed as approximately $3.92 \times 10^{-3} \text{ m}^2 \text{ s}^{-1}$ (Gregg et al., 2011). Diffusion in the current model is small ($10^{-7} \text{ m}^2 \text{ s}^{-1}$), thus mixing has an insignificant impact on nitrate flux calculations in the model simulations. Comparisons of estimated diffusive flux and model calculated advective flux provide true comparisons of the separate processes (Spurgin, 2014). In the upper 100 m, diffusion of nitrate is stronger than mean advection of nitrate. At 150 and 600 m, mean downwards advection of nitrate is stronger than upwards diffusion of nitrate. These positive diffusive flux estimates indicate that nitrate

Flow dynamics around downwelling submarine canyons

J. M. Spurgin and
S. E. Allen

Title Page

Abstract

Introduction

Conclusions

References

Tables

Figures

◀

▶

◀

▶

Back

Close

Full Screen / Esc

Printer-friendly Version

Interactive Discussion



- Boyer, D. L., Haidvogel, D. B., and Perenne, N.: Laboratory-numerical model comparisons of canyon flows: a parameter study, *J. Phys. Oceanogr.*, 34, 1588–1609, 2004. 1303
- Company, J. B., Ramirez-Llodra, E., Sarda, F., Aguzzi, J., Puig, P., Canals, M., Calafat, A., Palanques, A., Sole, M., Sanchez-Vidal, A., Martin, J., Lastras, G., Tecchio, S., Koenig, S., Fernandez-Arcaya, U., Mecho, A., and Fernandez, P.: Submarine canyons in the Catalan Sea (NW Mediterranean): megafaunal biodiversity patterns and anthropogenic threats, in: *Mediterranean Submarine Canyons: Ecology and Governance*, edited by: Wurtz, M., IUCN, Gland, Switzerland, Málaga, Spain, 133–144, 2012. 1303
- Dawe, J. T. and Allen, S. E.: Solution convergence of flow over steep topography in a numerical model of canyon upwelling, *J. Geophys. Res.-Oceans*, 115, C05008, doi:10.1029/2009JC005597, 2010. 1308
- Flexas, M. M., Boyer, D. L., Espino, M., Puigdefàbregas, J., Rubio, A., and Company, J. B.: Circulation over a submarine canyon in the NW Mediterranean, *J. Geophys. Res.-Oceans*, 113, doi:10.1029/2006JC003998, 2008. 1303, 1304, 1305, 1306, 1309, 1316, 1320, 1321, 1325, 1330, 1334
- Freeland, H. and Denman, K.: A topographically controlled upwelling center off southern Vancouver Island, *J. Mar. Res.*, 40, 1069–1093, 1982. 1303
- Gregg, M. C., Hall, R. A., Carter, G. S., Alford, M. H., Lien, R.-C., Winkel, D. P., and Wain, D. J.: Flow and mixing in Ascension, a steep, narrow canyon, *J. Geophys. Res.-Oceans*, 116, C07016, doi:10.1029/2010JC006610, 2011. 1329
- Griffies, S. M. and Hallberg, R. W.: Biharmonic friction with a Smagorinsky-like viscosity for use in large-scale eddy-permitting ocean models, *Mon. Weather Rev.*, 128, 2935–2946, 2000. 1307
- Hickey, B.: Coastal submarine canyons, in: *Topographic Effects in the Ocean*, SOEST Special publications, 95–110, 1995. 1303
- Jordi, A., Orfila, A., Basterretxea, G., and Tintoré, J.: Shelf-slope exchanges by frontal variability in a steep submarine canyon, *Prog. Oceanogr.*, 66, 120–141, 2005. 1304
- Klinck, J. M.: Circulation near submarine canyons: a modeling study, *J. Geophys. Res.-Oceans*, 101, 1211–1223, doi:10.1029/95JC02901, 1996. 1303, 1304, 1305, 1309, 1316, 1317, 1321, 1322, 1326, 1328, 1330, 1334
- Le Souëf, K. E. and Allen, S. E.: Physical modeling of tidal resonance in a submarine canyon, *J. Geophys. Res.-Oceans*, 119, 1324–1343, doi:10.1002/2013JC009612, 2014. 1303

Flow dynamics around downwelling submarine canyons

J. M. Spurgin and
S. E. Allen

Title Page

Abstract

Introduction

Conclusions

References

Tables

Figures

◀

▶

◀

▶

Back

Close

Full Screen / Esc

Printer-friendly Version

Interactive Discussion



Mann, K.: Overview of results, in: *Advances in Understanding the Gully Ecosystem: a Summary of Research Projects Conducted at the Bedford Institute of Oceanography (1999–2001)*, edited by: Gordon, D. and Fenton, D., Fisheries and Oceans Canada, Ottawa, p. 72, 2002. 1303

5 Orlanski, I.: A simple boundary condition for unbounded hyperbolic flows, *J. Comput. Phys.*, 21, 251–269, 1976. 1307

She, J. and Klinck, J. M.: Flow near submarine canyons driven by constant winds, *J. Geophys. Res.-Oceans*, 105, 28671–28694, doi:10.1029/2000JC900126, 2000. 1304, 1305, 1310, 1316, 1321, 1322, 1328, 1334

10 Skliris, N., Goffart, A., Hecq, J. H., and Djenidi, S.: Shelf-slope exchanges associated with a steep submarine canyon off Calvi (Corsica, NW Mediterranean Sea): a modeling approach, *J. Geophys. Res.-Oceans*, 106, 19883–19901, doi:10.1029/2000JC000534, 2001. 1303, 1304, 1305, 1309, 1316, 1317, 1321, 1322, 1326, 1328, 1330, 1334

15 Skliris, N., Hecq, J., and Djenidi, S.: Water fluxes at an ocean margin in the presence of a submarine canyon, *J. Marine Syst.*, 32, 239–251, 2002. 1303, 1304, 1305, 1316, 1317, 1321, 1322, 1326, 1328, 1330, 1334

Smagorinsky, J.: General circulation experiments with the primitive equations, *Mon. Weather Rev.*, 91, 99–164, doi:10.1175/1520-0493(1963)091<0099:GCEWTP>2.3.CO;2, 1963. 1307

20 Spurgin, J.: Flow dynamics around downwelling submarine canyons, Master's thesis, University of British Columbia, 2014. 1314, 1317, 1329

Flow dynamics around downwelling submarine canyons

J. M. Spurgin and
S. E. Allen

Table 1. Features seen in previous studies.

Study	Vorticity	Vertical Velocity	Temporal density change
Klinck (1996)	Positive everywhere	Net downwards (antisymmetrical)	Negative everywhere in canyon; positive on either side of the canyon
She and Klinck (2000)	Negative over the canyon, positive at 300 m	Net downwards	–
Skiris et al. (2001, 2002)	Positive everywhere	Net downwards (antisymmetrical)	Negative everywhere in canyon; positive on either side of the canyon
Flexas et al. (2008)	Negative over canyon, positive at 150 m	Net upwards	–

Title Page

Abstract

Introduction

Conclusions

References

Tables

Figures

◀

▶

◀

▶

Back

Close

Full Screen / Esc

Printer-friendly Version

Interactive Discussion



Flow dynamics around downwelling submarine canyons

J. M. Spurgin and
S. E. Allen

Title Page

Abstract

Introduction

Conclusions

References

Tables

Figures



Back

Close

Full Screen / Esc

Printer-friendly Version

Interactive Discussion



Table 2. Constant geometric parameters for model simulations.

Variable	Symbol	Value
Depth at shelf break	H_s [m]	150
Depth at canyon head*	H_h [m]	30
Depth drop across canyon	H_c [m]	950
Depth of basin	d [m]	1200
Canyon length	L [m]	16 180
Width at shelf break	W_{sb} [m]	13 005
Width at mid-canyon	W [m]	7660

* Value is different for Klinck-like simulation (KL), which used a flat shelf; $H_h = 150$ m.

Flow dynamics around downwelling submarine canyons

J. M. Spurgin and
S. E. Allen

Title Page

Abstract

Introduction

Conclusions

References

Tables

Figures

◀

▶

◀

▶

Back

Close

Full Screen / Esc

Printer-friendly Version

Interactive Discussion



Table 3. Non-dimensional parameters for all model simulations.

	Rosby number (R_o)	Burger number (B_u)	Stratification Uniformity (χ)
UW	0.22	0.46	-0.64
OW	0.25	0.46	-0.64
OBC	0.28	0.46	-0.64
ST	0.25	0.46	-0.64
KL	0.07	0.16	0
SK	0.04	0.14	-0.46
US	0.21	0.16	0
HB	0.28	0.46	0
She	0.04	0.28	-0.35
SF	0.05	0.46	-0.64
LRC	0.09	0.46	0
SHR	0.15	0.14	-0.46
BLRB	0.12	0.28	-0.63
KHRB	0.22	0.46	0

Flow dynamics around downwelling submarine canyons

J. M. Spurgin and
S. E. Allen

Title Page

Abstract

Introduction

Conclusions

References

Tables

Figures

◀

▶

◀

▶

Back

Close

Full Screen / Esc

Printer-friendly Version

Interactive Discussion



Table 4. Forcing flow for all model simulations.

	Jet location	Vertical shear	Horizontal shear
UW	outer shelf	surface intensified; negligible along bottom topography	intensified over mid-outer shelf to shelf break
OW	outer shelf	surface intensified; negligible along bottom topography	intensified over mid-outer shelf to shelf break
OBC	outer shelf	surface intensified; negligible along bottom topography; secondary jet at shelf break	intensified over shelf break
ST	outer shelf	surface intensified; negligible along bottom topography	intensified over mid-outer shelf to shelf break
KL	offshore	uniform offshore	uniform offshore of shelf break; weak flow over flat shelf (shelf break to coast)
SK	shelf break	intensified along bottom topography (150–600 m)	intensified between shelf break and 10 km offshore
US	offshore	intensified at shelf break depth (150 m); negligible along continental slope	intensified 5 km offshore of shelf break
HB	offshore	intensified at shelf break depth (150 m); negligible along continental slope	intensified 7 km offshore of shelf break
She	coastal	surface intensified	intensified near inner shelf
SF	coastal	surface intensified	intensified near inner shelf
LRC	offshore	intensified at shelf break depth (150 m); negligible along bottom topography	intensified 5 km offshore of shelf break
SHR	shelf break	intensified along bottom topography (150–600 m)	intensified between shelf break and 10 km offshore
BLRB	outer shelf	surface intensified; negligible along bottom topography	intensified over mid-outer shelf to shelf break
KHRB	offshore	uniform offshore; negligible along continental slope	uniform 10 km offshore of shelf break; weak flow over outer shelf; negligible over inner shelf

Flow dynamics around downwelling submarine canyons

J. M. Spurgin and
S. E. Allen

Title Page

Abstract

Introduction

Conclusions

References

Tables

Figures

◀

▶

◀

▶

Back

Close

Full Screen / Esc

Printer-friendly Version

Interactive Discussion



Table 5. Temporal variations in forcing for all model simulations.

	Wind magnitude (τ ; N m^{-2})	Peak body force magnitude (m s^{-1})	Constant body force magnitude (m s^{-1})
UW	0.0626	0.315	0.047
OW	0.0626 (offshore) 0.0376 (onshore)	0.315	0.063
OBC	0.13	0.53	0.133
ST	0.13	0.53	0.133
KL	–	0.06	0.024
SK	–	0.09	0.029
US	0.0626	0.315	0.079
HB	0.0626	0.315	0.047
She*	–	0.18	–
SF	0.0626	–	–
LRC	–	0.09	0.032
SHR	–	0.3	0.105
BLRB	0.0313	0.15	0.023
KHRB	–	0.18	0.063

Flow dynamics around downwelling submarine canyons

J. M. Spurgin and
S. E. Allen

Title Page

Abstract

Introduction

Conclusions

References

Tables

Figures

◀

▶

◀

▶

Back

Close

Full Screen / Esc

Printer-friendly Version

Interactive Discussion



Table 6. Absolute vorticity and canyon circulation for all model simulations.

	Absolute Vorticity* ($1/f$)	Canyon Circulation	Shelf break circulation
UW	−0.55	Anticyclonic (50–500 m)	Anticyclonic
OW	−0.54	Anticyclonic (0–500 m)	Anticyclonic
OBC	−0.50	Anticyclonic (75–400 m)	Anticyclonic
ST	−0.40	Anticyclonic (150–450 m)	Anticyclonic
KL	0.2	Cyclonic (0–400 m)	Cyclonic
SK	0.34	Cyclonic (all depths)	Cyclonic
US	0.97	Cyclonic (all depths)	Cyclonic
HB	−0.26	Cyclonic (200–500 m)	Anticyclonic
She	0.08	Cyclonic (all depths)	Weak
SF	0.07	Cyclonic (all depths)	Weak
LRC	−0.09	Anticyclonic (100–350 m)	Weak
SHR	0.71	Cyclonic (all depths)	Cyclonic
BLRB	−0.1	Anticyclonic (100–350 m)	Weak
KHRB	−0.14	Anticyclonic (100–300 m)	Anticyclonic

* Absolute vorticity is taken as maximum vorticity in the canyon head, away from canyon rims, at shelf break depth.

Flow dynamics around downwelling submarine canyons

J. M. Spurgin and
S. E. Allen

Title Page

Abstract

Introduction

Conclusions

References

Tables

Figures

◀

▶

◀

▶

Back

Close

Full Screen / Esc

Printer-friendly Version

Interactive Discussion



Table 7. Positive density and nitrate anomaly depth range for all model simulations. Pattern 1 anomalies had no positive values. Pattern 2 anomalies had positive values.

	Depth of positive density anomaly	Depth of positive nitrate anomaly	Jet location
UW	–	–	outer shelf
OW	–	–	outer shelf
OBC	–	50–200 m	outer shelf
ST	–	50–250 m	outer shelf
KL	surface to 200 m	50–200 m	offshore
SK	surface to 120 m	50–250 m	shelf break
US	surface to 100 m	25–200 m	offshore
HB	surface to 100 m	50–125 m	offshore
She	–	–	coastal
SF	–	–	coastal
LRC	surface to 150 m	75–125 m	offshore
SHR	surface to 100 m	25–250 m	shelf break
BLRB	–	–	outer shelf
KHRB	surface to 120 m	50–125 m	offshore

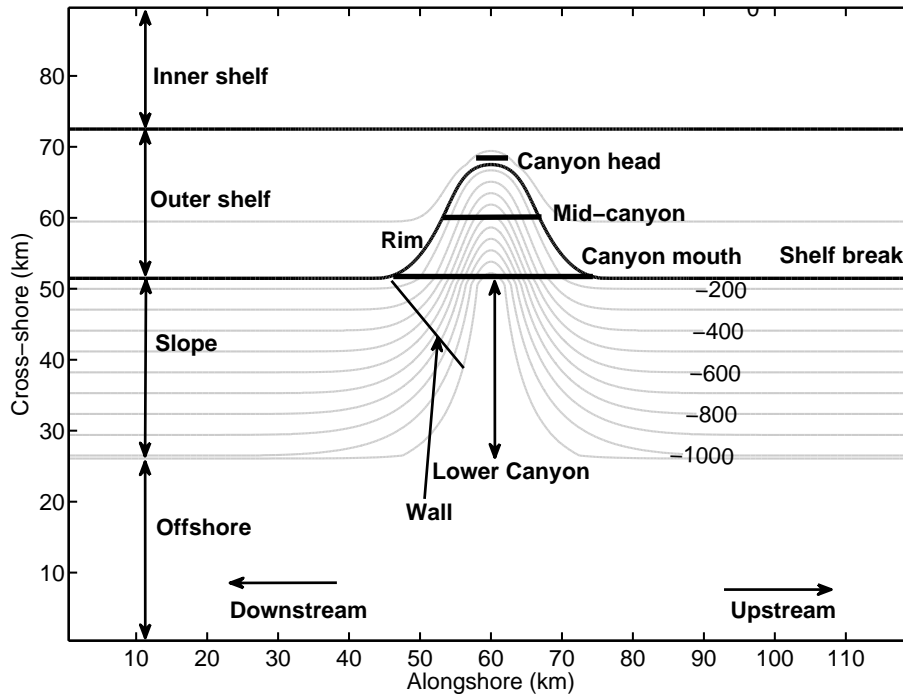


Figure 1. Canyon bathymetry (gray lines) and reference terminology used in this thesis. Canyon rim indicates the boundary between the continental shelf and the canyon. Shelf break indicates change in slope gradient between the continental shelf and slope. Canyon mouth is the open region along the shelf break; canyon head is the shallowest onshore canyon region; mid-canyon is the region between the canyon head and mouth; lower canyon is offshore of the canyon mouth. Canyon wall refers to canyon topography between shelf break and bottom depth. Zonal flow is in the alongshore, and meridional flow is in the cross-shore. Contour intervals are 100 m.

Flow dynamics around downwelling submarine canyons

J. M. Spurgin and
S. E. Allen

Title Page

Abstract

Introduction

Conclusions

References

Tables

Figures

◀

▶

◀

▶

Back

Close

Full Screen / Esc

Printer-friendly Version

Interactive Discussion



Flow dynamics around downwelling submarine canyons

J. M. Spurgin and
S. E. Allen

Title Page

Abstract

Introduction

Conclusions

References

Tables

Figures

◀

▶

◀

▶

Back

Close

Full Screen / Esc

Printer-friendly Version

Interactive Discussion

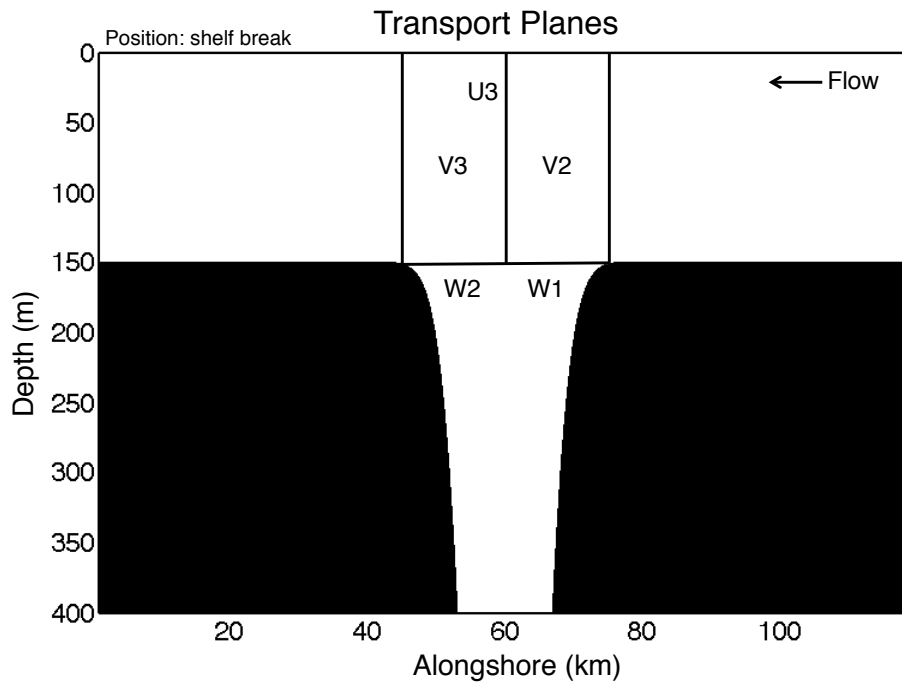


Figure 2. Planes used for transport calculations.

Flow dynamics around downwelling submarine canyons

J. M. Spurgin and
S. E. Allen

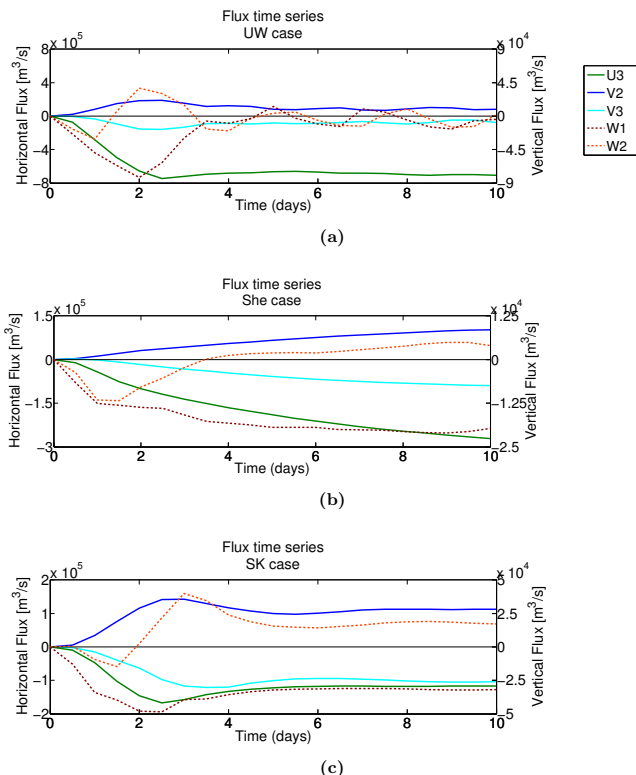


Figure 3. Time series of horizontal and vertical flux directly over the canyon for **(a)** core (UW), **(b)** surface forced (She) and **(c)** slope-current (SK) simulations. U3 indicates zonal flux across the canyon axis (from canyon head to canyon mouth). V2 and V3 are meridional flux along the canyon mouth from the upstream rim to canyon axis, and from the canyon axis to downstream rim, respectively. All horizontal fluxes are measured from surface to shelf break depth. W2 and W3 are vertical flux across the shelf break depth plane (150 m) everywhere within the canyon, from the upstream rim to canyon axis and from the canyon axis to downstream rim, respectively. Negative U, V, and W values indicate westward, offshore, and downwards fluxes.

Flow dynamics around downwelling submarine canyons

J. M. Spurgin and
S. E. Allen

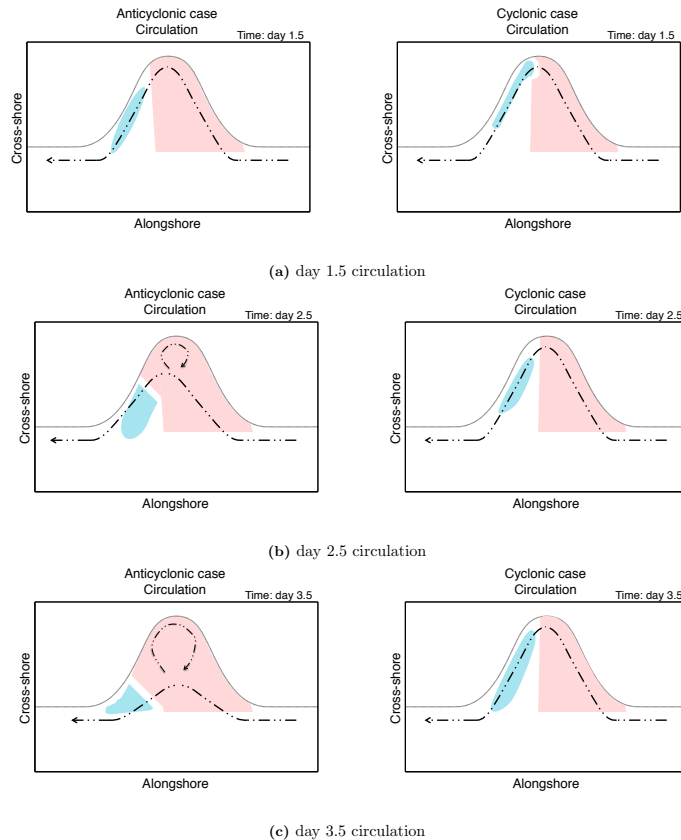
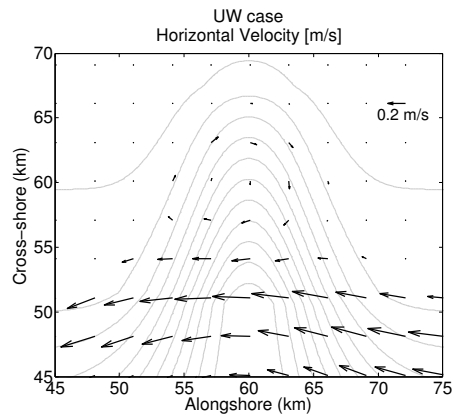


Figure 4. Horizontal and vertical circulation at shelf break depth during the time-dependent phase on **(a)** day 1.5, **(b)** day 2.5, and **(c)** day 3.5. Pink shading indicates downwards velocity and teal shading indicates upwards velocity. Circulation for a simulations with anticyclonic circulation (left) and cyclonic circulation (right) are shown.

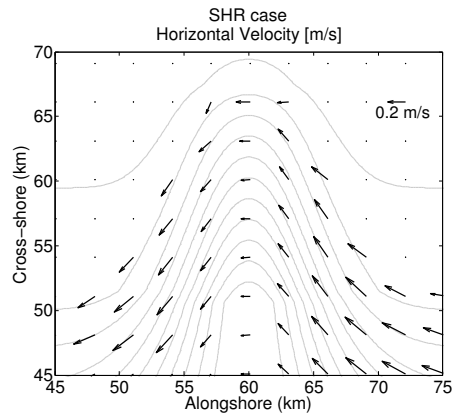
[Title Page](#)
[Abstract](#)
[Introduction](#)
[Conclusions](#)
[References](#)
[Tables](#)
[Figures](#)
[Back](#)
[Close](#)
[Full Screen / Esc](#)
[Printer-friendly Version](#)
[Interactive Discussion](#)

Flow dynamics around downwelling submarine canyons

J. M. Spurgin and
S. E. Allen



(a) Anticyclonic circulation



(b) Cyclonic circulation

Figure 5. Horizontal velocity vectors at shelf break depth (150 m) in **(a)** simulation with anticyclonic circulation (UW) and **(b)** simulation with cyclonic circulation (SHR). Vectors are averaged over a 3 model day period during the advection phase (model day 5–8).

Title Page

Abstract

Introduction

Conclusions

References

Tables

Figures

◀

▶

◀

▶

Back

Close

Full Screen / Esc

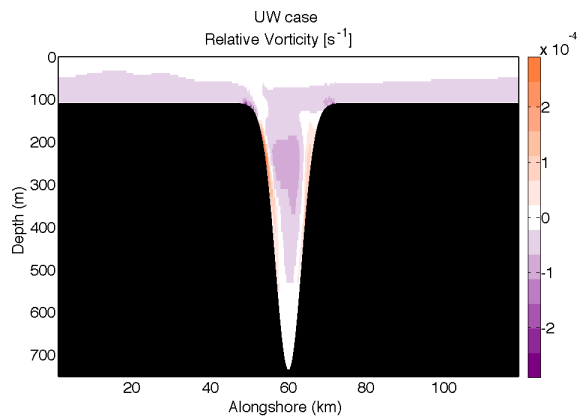
Printer-friendly Version

Interactive Discussion

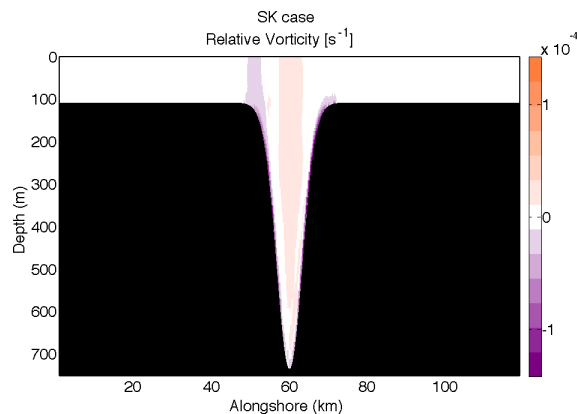


Flow dynamics around downwelling submarine canyons

J. M. Spurgin and
S. E. Allen

[Title Page](#)[Abstract](#)[Introduction](#)[Conclusions](#)[References](#)[Tables](#)[Figures](#)[Back](#)[Close](#)[Full Screen / Esc](#)[Printer-friendly Version](#)[Interactive Discussion](#)

(a) negative in canyon vorticity



(b) positive in canyon vorticity

Figure 6. Cross-section of vorticity at mid-canyon in (a) simulation exhibiting negative vorticity (UW) and (b) simulation exhibiting positive vorticity (SK).

Flow dynamics around downwelling submarine canyons

J. M. Spurgin and
S. E. Allen

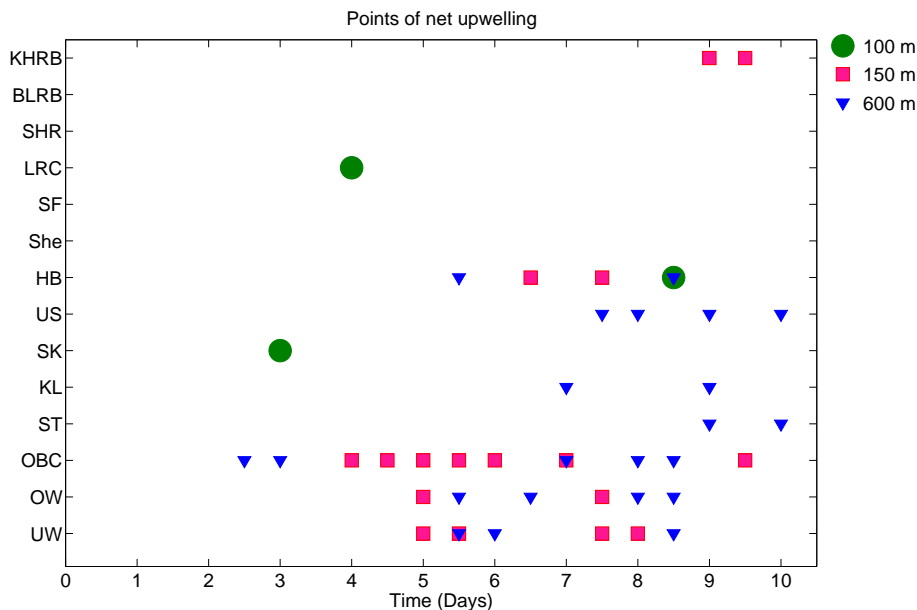


Figure 7. Times of net upwards flux across 3 vertical planes for all model simulations. Net upwards flux is plotted if larger than a minimum value of $1000 \text{ m}^3 \text{ s}^{-1}$.

[Title Page](#)
[Abstract](#)
[Introduction](#)
[Conclusions](#)
[References](#)
[Tables](#)
[Figures](#)
[◀](#)
[▶](#)
[◀](#)
[▶](#)
[Back](#)
[Close](#)
[Full Screen / Esc](#)
[Printer-friendly Version](#)
[Interactive Discussion](#)


Flow dynamics around downwelling submarine canyons

J. M. Spurgin and
S. E. Allen

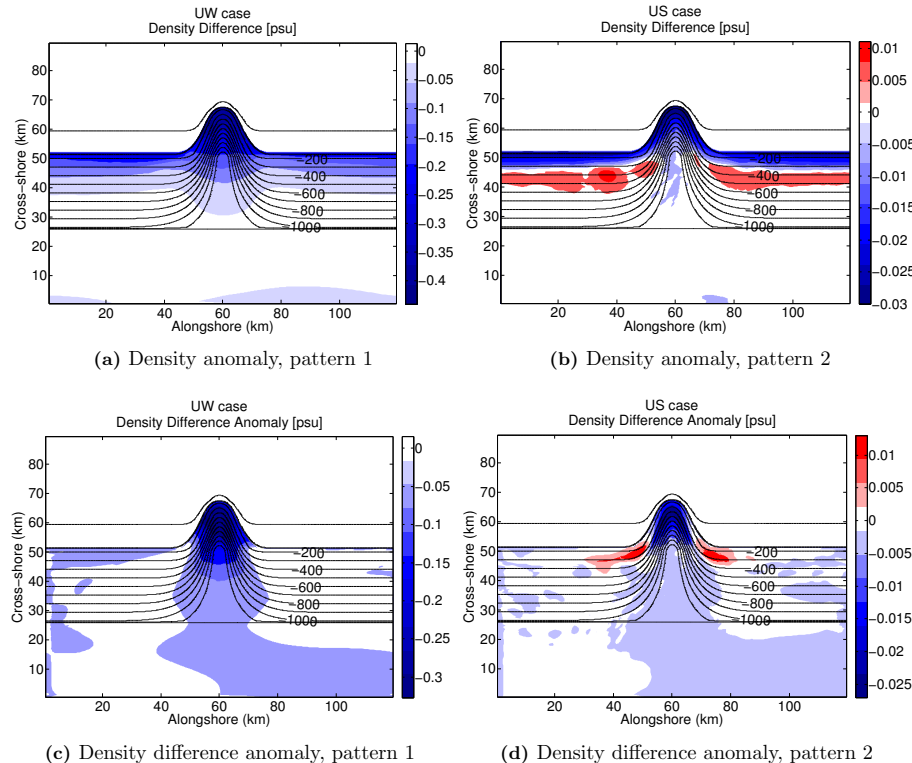


Figure 8. Density anomaly at shelf break depth (150 m) in **(a)** simulation with pattern 1: negative density anomalies at all depths (UW) and **(b)** simulation with pattern 2: positive density anomalies near the canyon (US). Density difference anomaly at shelf break depth (150 m) in **(c)** simulation with pattern 1: enhanced density advection everywhere in the model domain (UW) and **(d)** simulation with pattern 2: enhanced downwelling within the canyon and weaker downwelling near the canyon mouth (US).

Flow dynamics around downwelling submarine canyons

J. M. Spurgin and
S. E. Allen

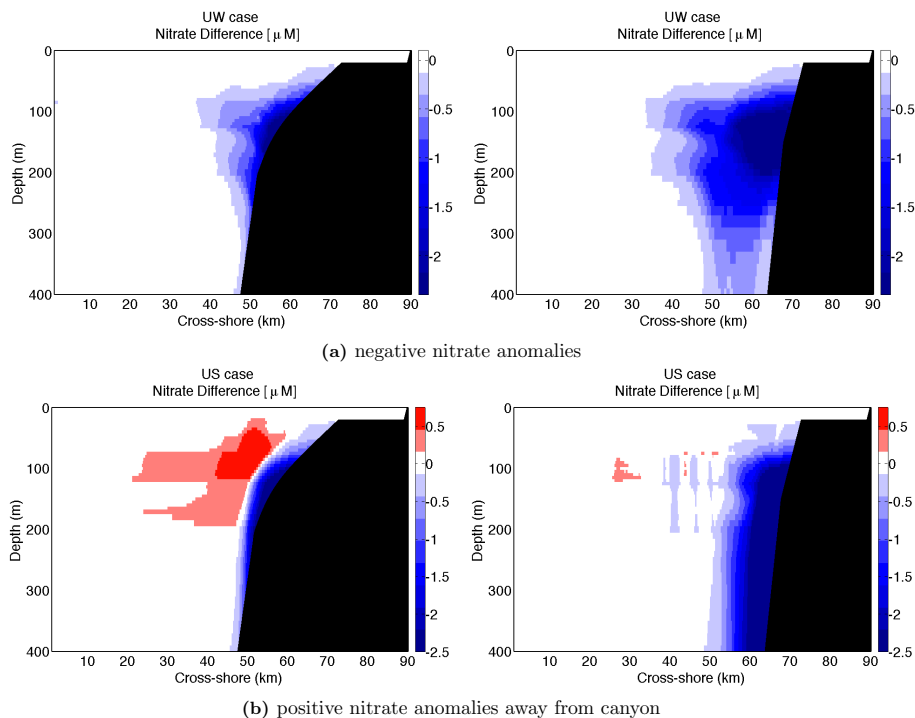


Figure 9. Nitrate anomaly 10 km upstream of canyon axis (left) and along canyon axis (right) in (a) simulation with pattern 1: negative nitrate anomalies at all depths (UW) and (b) simulation with pattern 2: positive nitrate anomalies near the canyon (US).

Title Page

Abstract

Introduction

Conclusions

References

Tables

Figures

◀

▶

◀

▶

Back

Close

Full Screen / Esc

Printer-friendly Version

Interactive Discussion



Flow dynamics around downwelling submarine canyons

J. M. Spurgin and
S. E. Allen

Title Page

Abstract

Introduction

Conclusions

References

Tables

Figures



Back

Close

Full Screen / Esc

Printer-friendly Version

Interactive Discussion

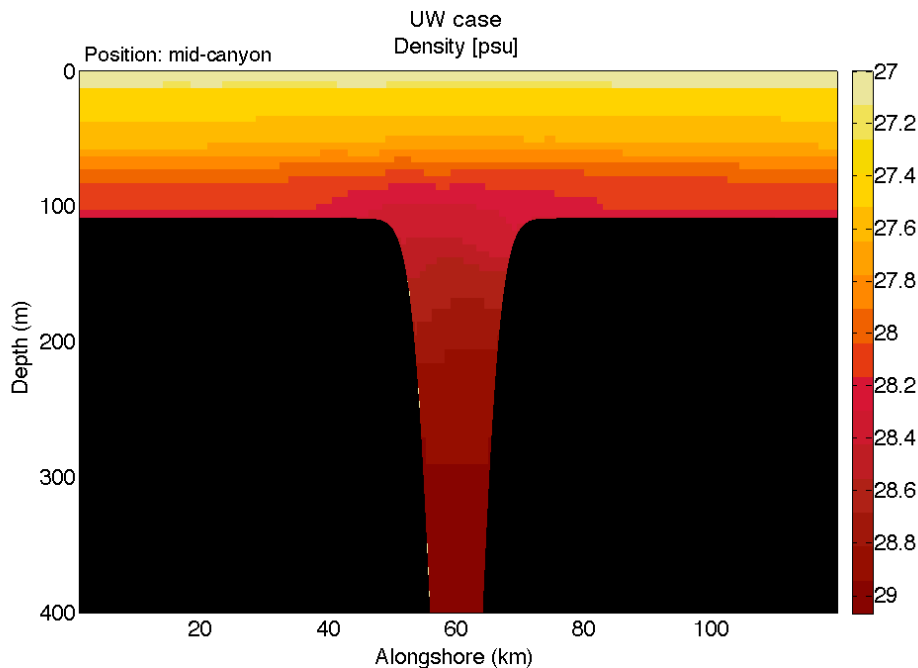
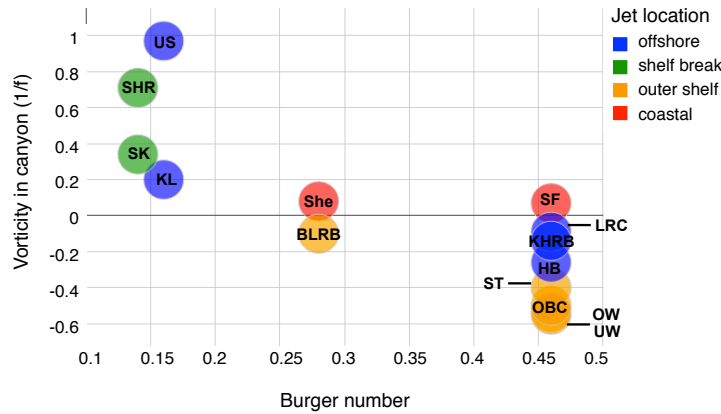


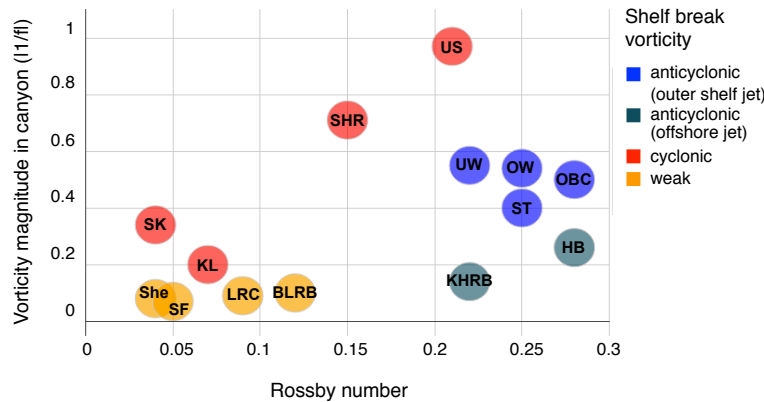
Figure 10. Isopycnal cross-section at mid-canyon in the core simulation (UW).

Flow dynamics around downwelling submarine canyons

J. M. Spurgin and
S. E. Allen



(a)



(b)

Figure 11. Effect of (a) Burger number and (b) incoming Rossby number on canyon vorticity for all model simulations.

Title Page

Abstract

Introduction

Conclusions

References

Tables

Figures

◀

▶

◀

▶

Back

Close

Full Screen / Esc

Printer-friendly Version

Interactive Discussion



Flow dynamics around downwelling submarine canyons

J. M. Spurgin and
S. E. Allen

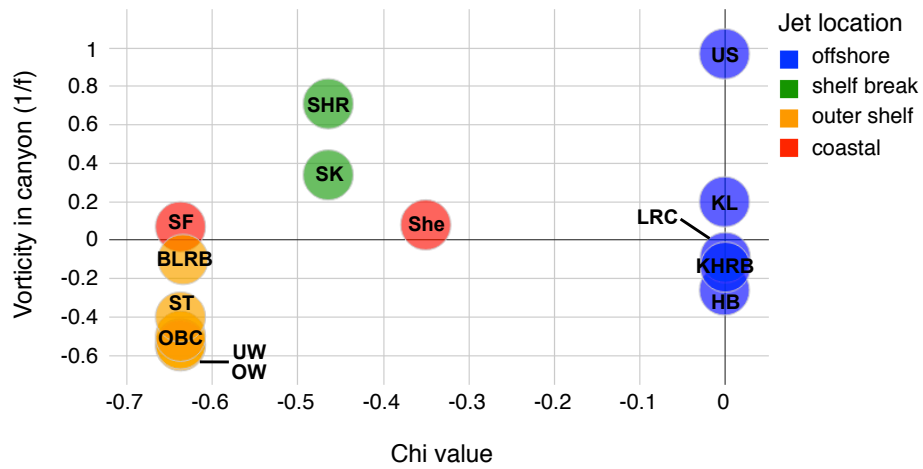


Figure 12. Zonal jet location upstream of the canyon.

Title Page	
Abstract	Introduction
Conclusions	References
Tables	Figures
◀	▶
◀	▶
Back	Close
Full Screen / Esc	
Printer-friendly Version	
Interactive Discussion	



Flow dynamics around downwelling submarine canyons

J. M. Spurgin and
S. E. Allen

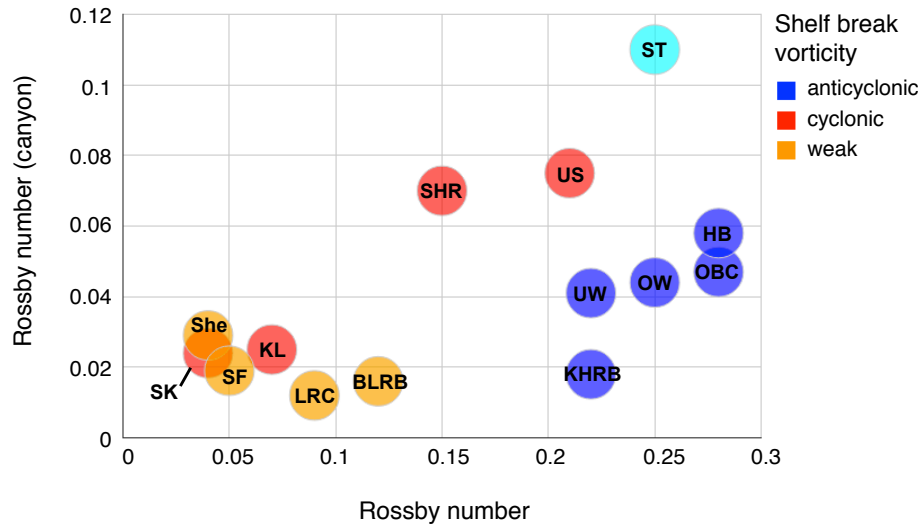


Figure 13. Correlation between Rossby numbers based on incoming zonal flow and zonal flow integrated across the canyon axis. Due to complex canyon topography, canyon Rossby number for ST is likely overestimated and ST is considered an outlier.

Title Page

Abstract Introduction

Conclusions References

Tables Figures

◀ ▶

◀ ▶

Back Close

Full Screen / Esc

Printer-friendly Version

Interactive Discussion



Flow dynamics around downwelling submarine canyons

J. M. Spurgin and
S. E. Allen

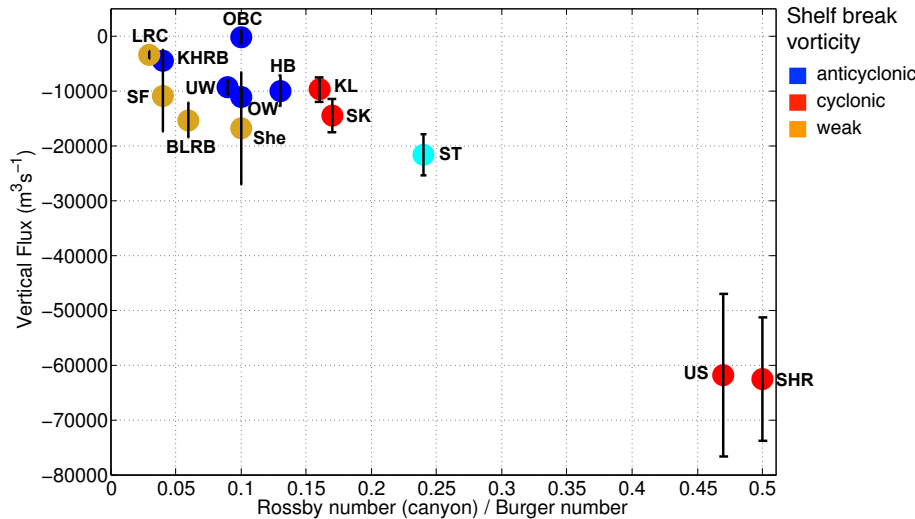


Figure 14. Burger and canyon Rossby number effect on vertical flux at shelf break depth (150 m). Due to complex canyon topography, canyon Rossby number for ST is likely overestimated and ST is considered an outlier.

Title Page

Abstract Introduction

Conclusions References

Tables Figures

◀ ▶

◀ ▶

Back Close

Full Screen / Esc

Printer-friendly Version

Interactive Discussion



Flow dynamics around downwelling submarine canyons

J. M. Spurgin and
S. E. Allen

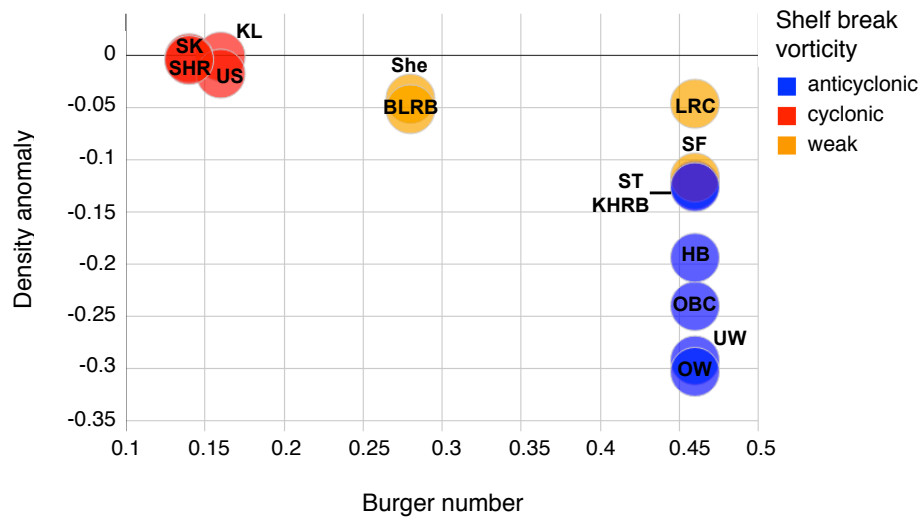


Figure 15. Burger number effect on average density anomaly in canyon for all simulations (averaged between model days 4–10).

Title Page

Abstract Introduction

Conclusions References

Tables Figures

◀ ▶

◀ ▶

Back Close

Full Screen / Esc

Printer-friendly Version

Interactive Discussion



Flow dynamics around downwelling submarine canyons

J. M. Spurgin and
S. E. Allen

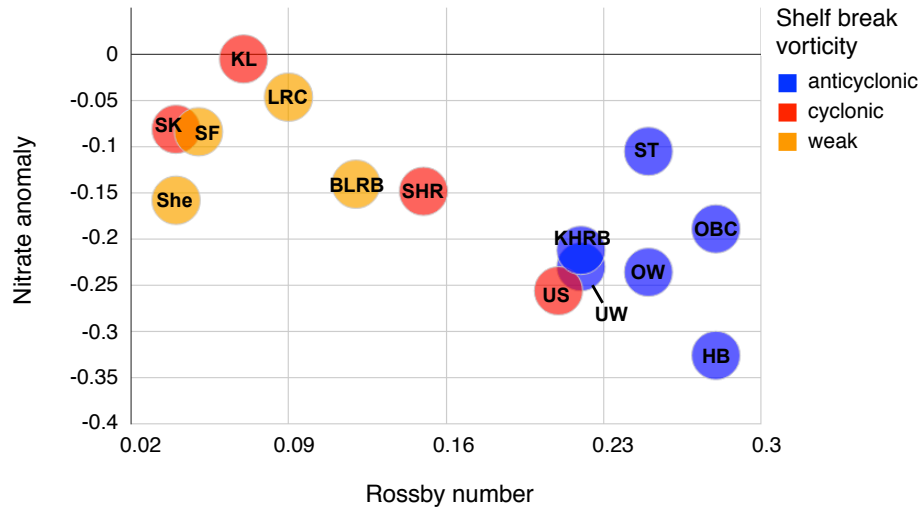


Figure 16. Incoming Rossby number effect on nitrate anomaly for all simulations (averaged between model days 4–10).

Title Page

Abstract

Introduction

Conclusions

References

Tables

Figures

◀

▶

◀

▶

Back

Close

Full Screen / Esc

Printer-friendly Version

Interactive Discussion

